Analytical Methods

ROYAL SOCIETY OF CHEMISTRY

PAPER

View Article Online
View Journal

Cite this: DOI: 10.1039/d6ay00361c

Electrochemically amplified nanozymatic activity of biolinker-based Co-MOF for H_2O_2 and dopamine detection

Jasmine Look,[a] Syed Rahin Ahmed, *[a] Mohamed Hassan Mahana,[bc] Md. Shalauddin,*[d] Shamima Akhter,*[e] Wan Jefrey Basirun, *[fg] Seshasai Srinivasan *[ab] and Amin Reza Rajabzadeh *[ab]

Rapid, sensitive and selective H_2O_2 and dopamine sensors provide enormous opportunities to health, food and environmental monitoring, which could prevent major social and economic losses. To overcome the sluggish response and low sensitivity of the conventional colorimetric assays, an electrochemical platform integrated with the conventional assay was proposed in this work. First, a microwave-assisted cobalt MOF (Co-MOF) was synthesized using a bio-linker and characterized using FESEM and TEM. The electrochemical performance of Co-MOF was examined through cyclic voltammetry (CV), where eight-fold higher currents were achieved for Co-MOF compared to those of the unmodified electrode. However, Co-MOF exhibits very weak nanozymatic activity in a mixture of 3,3′,5,5′-tetramethylbenzidine (TMB) and H_2O_2. Integration of the superior electrochemical characteristics of Co-MOF with the nanozymatic activity resulted in a six-fold enhanced nanozymatic activity that enabled H_2O_2 quantification with a limit of detection (LOD) of 32 nM under optimized conditions. The modified electrode was further used to quantify dopamine, achieving an LOD of 0.81 μM, with a remarkably shorter detection time (60 fold shorter) compared to the conventional nanozyme. A mechanistic study showed that Co-MOF provides a large surface area and abundant redox-active sites, facilitating fast electron transfer and significantly enhancing the electrochemical signal.

Received 1st March 2026
Accepted 22nd April 2026

DOI: 10.1039/d6ay00361c

rsc.li/methods

Introduction

Metal–organic frameworks (MOFs) are crystalline and porous polymers assembled from metal ions and organic linkers. They have many unique properties, including high porosity, large surface area, excellent thermal and chemical stability, and many active sites. These qualities have made them attractive in many applications such as chemical sensing, gas and energy storage, separation, catalysis, luminescence, and drug delivery.[1–7] Though several research studies have been reported on the nanozymatic activity of MOFs, most of them have discussed the specific type of MOFs showing nanozymatic activity. There have been no reports on the current challenges associated with the weak nanozymatic activity of MOFs, possible ways to improve their properties and their future perspectives.

Nanozymes have shown tremendous development in recent years due to their ability to catalyze reactions similar to natural enzymes while overcoming their drawbacks, such as low stability under varying temperatures, low durability, high cost, and strict storing conditions. Nanozymes offer an opportunity to overcome those drawbacks of natural enzymes. To date, a large number of nanomaterials with enzyme-mimicking characteristics have been discovered. Remarkably, it has been observed that a wide range of nanomaterials simultaneously display dual- or multi-enzyme resembling activity.[8–15] In comparison to natural enzymes, nanozymes possess higher catalytic stability, are easier to modify, and are more affordable for mass production. Their catalytic activity can be easily regulated by modifications to their size, structure, or surface. In addition to their enzyme-like activity, nanozymes demonstrate several other properties, such as fluorescence, superparamagnetism, and optical absorption that might be helpful for multiple applications. These unique properties of nanozyme

[a]W Booth School of Engineering Practice and Technology, McMaster University, 1280 Main Street West Hamilton, Ontario, L8S 4L7, Canada. E-mail: ahmes91@mcmaster.ca; ssriniv@mcmaster.ca

[b]School of Biomedical Engineering, McMaster University, 1280 Main Street West Hamilton, Ontario, L8S 4L7, Canada. E-mail: rajaba@mcmaster.ca

[c]Department of Pharmaceutical Analytical Chemistry, Faculty of Pharmacy, Tanta University, Tanta 3111, Egypt

[d]School of Pharmacy, Faculty of Health and Medical Sciences, Taylor's University, Subang Jaya, Selangor 47500, Malaysia. E-mail: md.shalauddin@taylors.edu.my

[e]Department of Pharmaceutical Chemistry, School of Pharmacy, IMU University, Bukit Jalil, 57000 Kuala Lumpur, Malaysia. E-mail: shamimaakhter@imu.edu.my

[f]Nanotechnology and Catalysis Research Center (NANOCAT), University Malaya, 50603 Kuala Lumpur, Malaysia

[g]Department of Chemistry, Faculty of Science, University Malaya, 50603 Kuala Lumpur, Malaysia. E-mail: jeff@um.edu.my

have enabled a broad range of applications, such as in *in vitro* detection, *in vivo* disease monitoring, drug delivery and replacement of certain natural enzymes in living systems, and most notably in biotechnology research.[16–22]

The ability of enzyme-integrated MOF nanozymes to function as stable enzyme supports and catalyze cascade reactions in a single step has also made them prominent in biosensing and biocatalysis applications. A few mono- and bi-metallic MOFs have been reported to exhibit outstanding oxidase, peroxidase, catalase, and superoxide dismutase-like activities.[6]

Recent reports on the inherent nanozyme activity of Co-MOF have made it possible for a selective, stable, and sensitive biosensing of glucose and H_2O_2, establishing it as an effective nanozyme and enzyme support.[6] Co-MOF is also an excellent colorimetric sensing catalyst for phosphate detection. The nanomaterial acts as a catalytic chromogenic platform for phosphate ions (Pi), which in excess could negatively impact the body's ability to absorb minerals and result in detrimental health issues.[23] Yuwei and co-workers reported a Co-based multifunctional nanozyme with increased catalytic active sites, which was applied for the detection of environmental phenolic pollutants and disease identification.[24] Further modifications and additional component materials to the nanohybrid Co-MOF elevated its functionalities. For example, the increase in electrical conductivity of the Co-MOF-74-TTF nanocomposite is useful for atmospheric gas adsorption and could be used in gas sensing.[7] Junwen and co-workers have presented a bimetallic copper/cobalt-doped nanozyme (Cu-Co-NC) for the dual-mode dopamine detection.[25] However, to the best of our knowledge, there have been no reports on the use of the electrical conductivity of Co-MOF to enhance its nanozymatic activity for biosensing applications. Furthermore, the integration of both electrochemical and colorimetric techniques into a unified platform offers more advantages than employing either method independently. This combination provides enhanced sensitivity, dependability, and portability by facilitating cross-verification of results, thereby minimizing the occurrence of false positives and negatives typically associated with single-mode systems.

Hydrogen peroxide (H_2O_2), a reactive oxygen species, is widely present throughout the body and plays diverse roles in physiological processes, including cellular communication, which controls immunological activation, cell proliferation, and apoptosis. However, excessive amounts of H_2O_2 may be harmful to the body, resulting in cancer, inflammatory diseases, and cell damage.[26] The reactivity and low concentration of H_2O_2 in the body make reliable detection challenging.

Moreover, dopamine concentrations in the brain are associated with various diseases. For example, the decrease of dopamine in the brain produces neurons that cause Parkinson's disease, while the excess amount of dopamine is related to schizophrenia.[25] Hence, an accurate detection system of H_2O_2 and dopamine at low concentration levels is important for a quick diagnosis, to examine the disease progression and estimation of therapeutic efficiency.

The present study aims to examine the electrical nature of newly synthesized Co-MOF and apply the electrical properties of Co-MOF to improve its nanozymatic activity. The proposed nanozymatic activity enhancement strategy is much simpler than the other techniques, namely, ligand-based enhancement, hybrid nanozyme, nanomaterials size, shape or charge dependent nanozymatic activity enhancements.[11,12,16]

In this study, the electrical conductivity of Co-MOF was utilized to enhance the nanozymatic activity. In general, the nanozymatic activity of nanomaterials is performed on well plates or in microtubes in the presence of TMB and H_2O_2. In this study, we performed all the nanozymatic reactions under electrochemical conditions to achieve higher sensitivity and shorter detection times. We introduced a new synthesis route of Co-MOF using 2,5-furandicarboxylic acid, a bio-based linker (Scheme 1). Subsequently, we utilized the as-synthesized Co-MOF for the detection of H_2O_2 and dopamine through its electro-nanozymatic activity.

Materials and methods

Materials

Hydrogen peroxide (H_2O_2), sodium acetate, cobalt nitrate hexahydrate, 2,5-furandicarboxylic acid, 3,3′,5,5′-tetramethylbenzidine (TMB), tablet of phosphate-buffered saline (PBS), dopamine hydrochloride, dimethylformamide (DMF) and dimethyl sulfoxide (DMSO), and ethanol were obtained from Sigma-Aldrich (Canada).

Synthesis of cobalt MOF

Co-MOF was synthesized through a microwave-assisted method following a previous report,[1] with a slight modification in the synthesis procedure. Firstly, 0.4366 g of cobalt nitrate hexahydrate $Co(NO_3)_2 \cdot H_2O$ as the initial material, 0.3634 g of 2,5-furandicarboxylic acid as the linker and 40 mL of DMF were mixed in a beaker and stirred for 20 min to produce a homogeneous dispersion. Then, the dispersion was irradiated in a microwave at 200 °C, 600 W for 45 min to obtain a solid precipitate. A deep purple coloured precipitate was obtained, which was washed with suction filtration with ethanol to remove impurities. The product was dried at 60 °C in a microwave oven to obtain the Co-MOF powder.

Optimization of Co-MOF concentration

The optimization of Co-MOF concentration was performed over the range of 0 to 70 μg mL^{-1} while the TMB and H_2O_2 concentrations were kept unchanged. The concentration of Co-MOF, which gave the highest absorbance, represents the best concentration in this study.

TMB optimization

The optimization of the TMB concentration involved the preparation of TMB solutions with different concentrations and their examination at a fixed concentration of H_2O_2, reaction time, and Co-MOF concentration. Here, the TMB concentration ranged from 1 to 8 mM with an interval of 1 mM. The concentration of H_2O_2 and Co-MOF was 10 μM and 70 μg mL^{-1}, respectively. The reaction was performed at room temperature for 30 min.

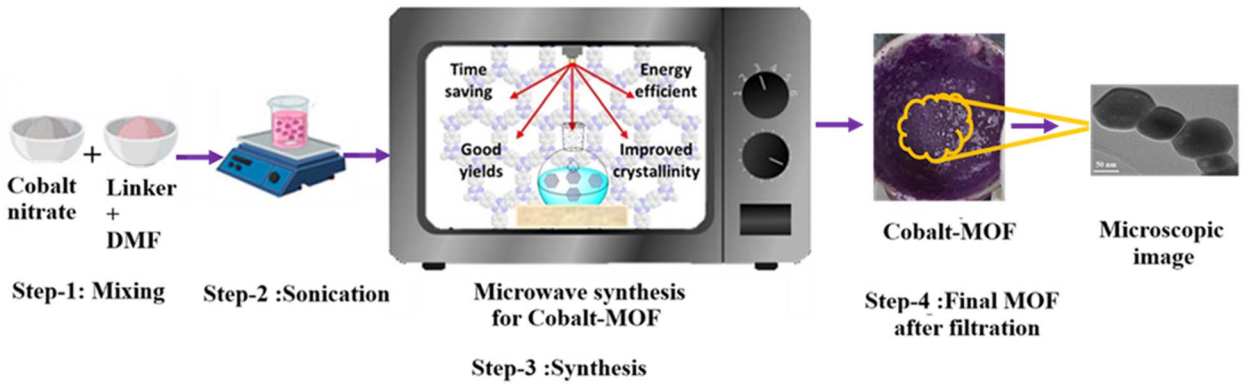

Scheme 1 Microwave-assisted synthesis procedure of Co-MOF.

Optimization of pH and reaction time

The optimization of pH was performed in sodium acetate buffer (pH 5.2) and PBS buffer (pH 7.4), while keeping the concentration of TMB, H_2O_2 and Co-MOF constant throughout the experiment.

The reaction time was also monitored carefully by data collection for 40 seconds with a 5 second time interval. The time required for the concentrated blue solution to achieve the maximum absorbance peak represents the optimum reaction time.

H_2O_2 detection

Upon completion of the optimization steps, the detection of H_2O_2 was performed through the proposed detection method as well as the conventional method. For the conventional assay, 0.1 mL of the Co-MOF (40 μM) solution was added to the TMB solution (1 mL, 6 mM) in a microplate. Then, 50 μL of different concentrations (1–10 μM) of H_2O_2 was added separately. After 30 min of the reaction, the absorbance of the blue color solution of each well was recorded, and a calibration curve of absorbance *vs.* concentration of H_2O_2 was constructed.

The cyclic voltammetry (CV) analysis on a glassy carbon electrode (GCE) was used to investigate the electro-nanozymatic process for the detection of H_2O_2 over a range of −1 V to 1 V with a scan rate of 0.1 V s^{-1}. A UV-visible spectrometer (BioTek) was used to record the absorbance of the solution upon the appearance of a blue color within 30 seconds.

Dopamine detection

At first, Co-MOF, TMB, H_2O_2, and 5 μL of different concentrated dopamine hydrochloride solutions (2–12 μM) were added separately to quantify dopamine. A UV-visible spectrometer was used to record the absorbance of the solution upon turning blue within 30 seconds.

Kinetic assessment of TMB and H_2O_2

The kinetic parameters of Co-MOF were assessed by varying the concentrations of TMB and H_2O_2. The concentration range of TMB was 0–10 mM while the concentration of H_2O_2 was fixed at 10 μM. The concentration of H_2O_2 was selected within the range 0–10 μM while the concentration of TMB was maintained constant at 10 mM. The results were then transformed into initial velocities based on our recent article.[27] Then, the Michaelis–Menten constant (K_m) and the maximum reaction rate (V_{max}) were calculated from the Michaelis–Menten and Lineweaver–Burk plots.

Electrochemical measurements

A PalmSens4 potentiostat (EmStat-MUX8-R2) multiplexer was used for electrochemical measurements, while a Zensor glassy carbon electrode (GCE) was the electrode and PBS at pH 7 as the electrolyte. For electrochemical measurements, 2 mg of Co-MOF was first dispersed in 2 mL of ethanol and sonicated for 15 minutes to obtain a uniform suspension. Subsequently, 5 μL of the suspension was drop-cast onto a bare glassy carbon electrode (GCE) and allowed to dry at room temperature. After drying, the modified GCE was used for electrochemical analysis.

Results and discussions

The morphological features of Co-MOF were characterized by FESEM, TEM and EDX. As shown in Fig. 1A (FESEM image), Co-MOF appears as a granular pearl-shaped and distributed evenly on the surface. The TEM image (Fig. 1B) reveals that the synthesized Co-MOF consists of closely aggregated quasi-spherical particles, forming interconnected structures. The particle size is in the nanometer range, indicating successful nanoscale formation. High-resolution TEM (Fig. 1C) clearly shows lattice fringes with *d*-spacings of 1.34 nm, 1.21 nm, and 1.15 nm, which can be indexed to the (200), (001), and (201) crystallographic planes, respectively. These well-defined lattice fringes confirm the crystalline nature of the material at the nanoscale.

The SAED pattern (Fig. 1D) displays a series of concentric diffraction rings, indicating that the material is polycrystalline with randomly oriented nanocrystallites. The appearance of rings rather than discrete spots suggests the presence of multiple crystalline domains contributing to the diffraction. The ring positions are consistent with the (200), (001), and (201) planes, which correlate well with the XRD results, confirming

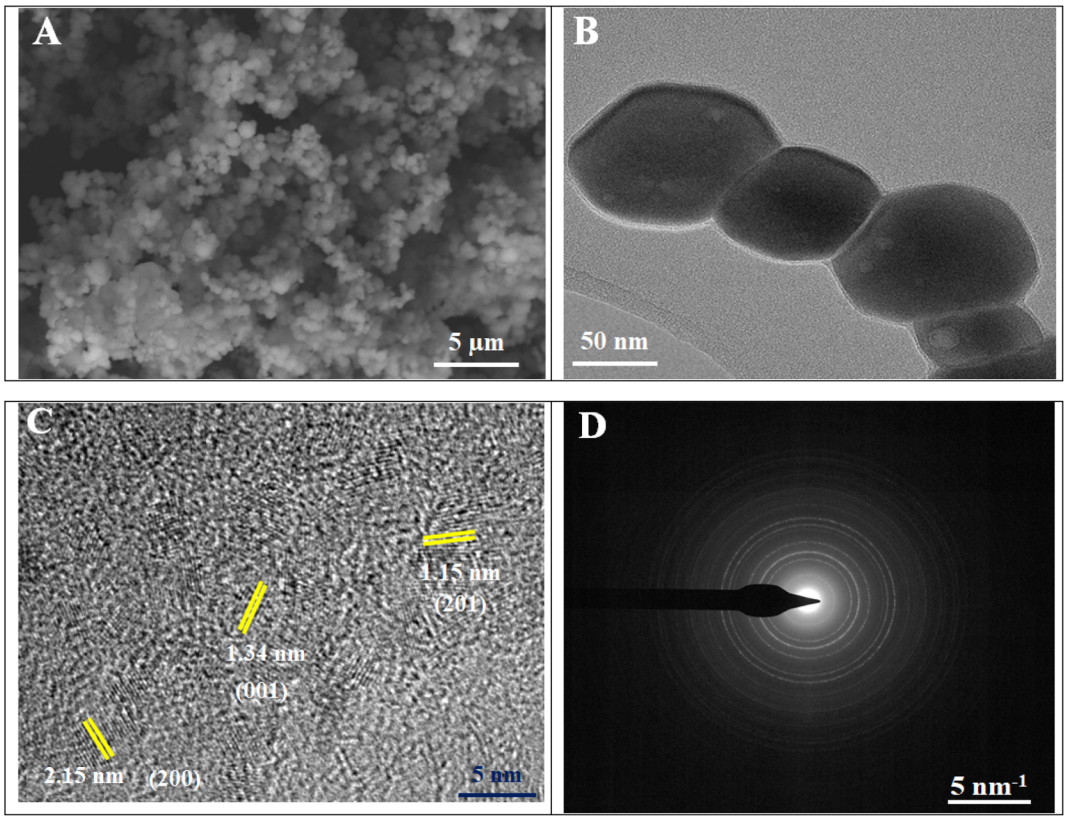

Fig. 1 FESEM analysis for Co-MOF nanoparticles (A) TEM analysis for Co-MOF nanoparticles (B) lattice spacings for Co-MOF nanoparticles (C) and SEAD pattern for Co-MOF nanoparticles (D).

structural agreement between nanoscale and bulk characterization.

EDX analysis (from FESEM) shows the percentage of major elements C, O, N and Co as 40.61%, 51%, 8.39%, respectively, indicating all the main elements are present in Co-MOF (Fig. S1).

The FTIR spectrum of the synthesized material (Fig. 2A) exhibits several characteristic bands confirming the formation of the Co-based framework. The absorption bands at ~590 cm^{-1} and 660 cm^{-1} are assigned to Co–O stretching vibrations, indicating the coordination between cobalt ions and the oxygen atoms of the carboxylate groups of 2,5-furandicarboxylic acid. These bands fall within the typical range reported for metal-carboxylate vibrations in Co-based metal–organic frameworks (500–700 cm^{-1}).[28,29]

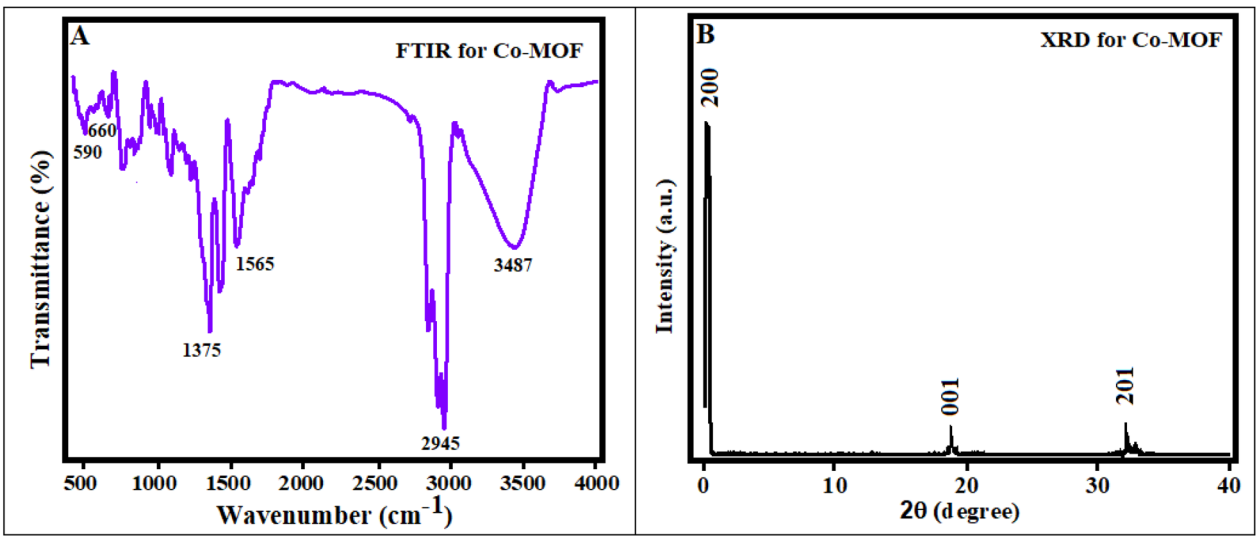

Fig. 2 FTIR spectra of Co-MOF nanoparticles (A). XRD analysis of Co-MOF nanoparticles (B).

For comparison, a Co–N vibration at ~442 cm^{-1} has been reported in a previous study,[30] which is associated with cobalt coordinated to nitrogen-containing ligands. However, such a feature is not observed in the present study. This is expected because the current system does not involve nitrogen donors; instead, cobalt coordination occurs predominantly through oxygen atoms of the carboxylate groups. In addition, the FTIR spectrum recorded in this work does not extend below 500 cm^{-1}, where the Co–N vibration is typically detected.

Furthermore, the peaks at 1565 cm^{-1} and 1375 cm^{-1} correspond to the asymmetric and symmetric stretching vibrations of the coordinated carboxylate ($-COO^-$) groups, confirming ligand–metal interactions. The band at 2945 cm^{-1} is attributed to C–H stretching vibrations, while the broad peak at 3487 cm^{-1} is assigned to the O–H stretching, likely arising from adsorbed moisture or residual hydroxyl groups. These observations collectively support the successful formation of the Co-carboxylate framework.[31]

The XRD pattern of the synthesized Co-MOF (Fig. 2B) shows distinct diffraction peaks, confirming its crystalline nature. The characteristic peaks observed at 2.5°, 19.4°, and 32.5° can be indexed to the (200), (001), and (201) planes, respectively. These diffraction peaks are in good agreement with the standard JCPDS data (No. 15-0806), confirming phase purity and successful formation of the framework.[32]

Notably, these crystallographic planes are consistent with the lattice spacings obtained from HRTEM and the ring patterns observed in SAED, demonstrating strong agreement between bulk (XRD) and local (TEM/SAED) structural analyses.

Cyclic voltammetry (CV) was conducted to observe the electrochemical characteristics of a bare glassy carbon electrode (GCE) and Co-MOF/GCE. As depicted in Fig. 3A, at 0.5 V s^{-1} and pH 7, the unmodified GCE demonstrates a low current response of 3 μA, indicative of slow interfacial charge-transfer kinetics. In contrast, Co-MOF/GCE exhibits a significantly higher current response within the measured range of 25 μA, suggesting a strong interaction between the expanded surface area of Co-MOF and the ionic species present in the buffer solution. The current response of Co-MOF/GCE is approximately eight-folds higher compared to the unmodified GCE. This increased surface area enhances charge-transfer efficiency and electrical conductivity, thereby leading to significant electrochemical performance of the Co-MOF/GCE electrode in comparison to the unmodified GCE.

Linear sweep voltammetry (LSV) of GCE and Co-MOF/GCE is presented in Fig. 3B at 0.5 V s^{-1} with 0.5 mM KOH. The

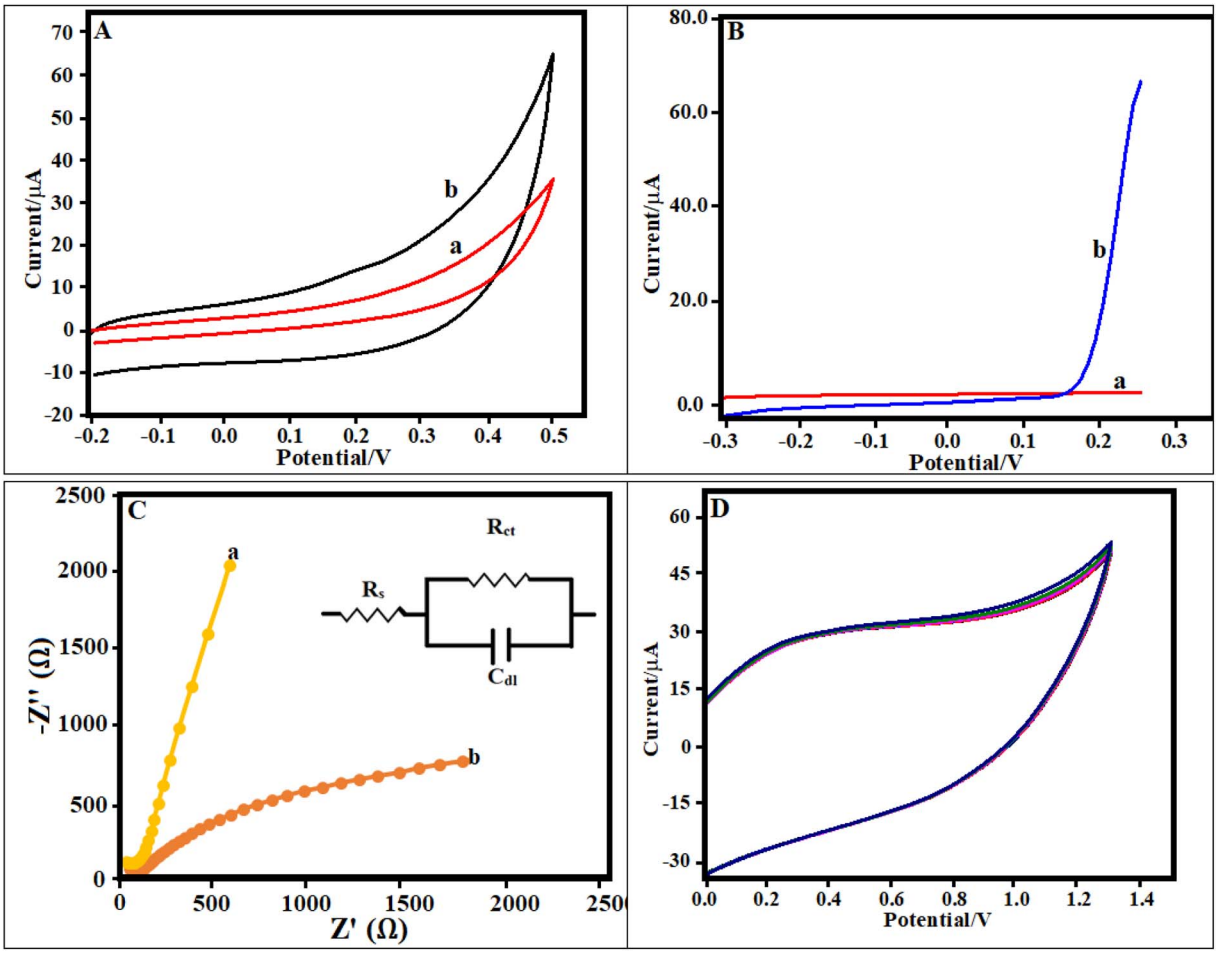

Fig. 3 CV analysis for Co-MOF nanoparticles at 0.5 V s^{-1} at pH 7 (A) LSV for Co-MOF nanoparticles at 0.5 V s^{-1} using 0.5 mM KOH (B) Nyquist plot from EIS analysis of Co-MOF nanoparticles (C) (inset: circuit diagram) and CV of Co-MOF nanoparticles at 0.5 V s^{-1} at pH 7 (D).

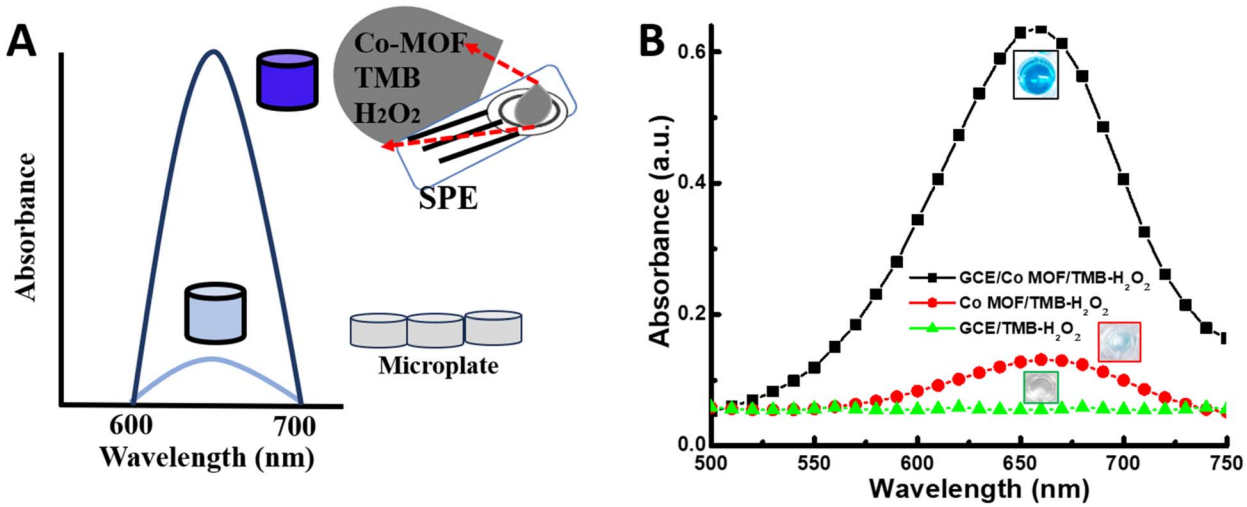

Fig. 4 Schematic of the modified nanozymatic activity (A) and experimental results of the proposed nanozymatic activity (B).

unmodified GCE (curve a) exhibits a very low current response at curve a (~2 μA), whereas Co-MOF/GCE shows a significantly enhanced current at curve b (~71.4 μA) at a potential range of approximately 0.2–0.3 V. This pronounced increase in current is attributed to improved electron-transfer kinetics and the higher electroactive surface area of the Co-MOF-modified electrode, rather than the oxygen evolution reaction (OER), which typically occurs at much higher potentials.

Electrochemical impedance spectroscopy (EIS) was performed in 1.0 mM thiourea containing 0.1 M phosphate-buffered saline (PBS) with an amplitude of 10 mV over a frequency range of 10^{-2} to 10^{5} Hz (Fig. 3C). The Nyquist plots exhibit a semicircular feature in the high-frequency region, corresponding to the charge transfer resistance (R_{ct}), while no well-defined linear Warburg diffusion region is observed at low frequencies. This indicates that the electrochemical process is predominantly controlled by charge transfer rather than diffusion. The extracted R_{ct} values are 598.36 Ω for the bare GCE and 121.47 Ω for Co-MOF/GCE, confirming significantly enhanced electron-transfer kinetics at the modified electrode. The smaller diameter of the semicircle for Co-MOF/GCE reflects its higher electrical conductivity and improved electroactive surface properties. The impedance data were fitted using an equivalent circuit consisting of solution resistance (R_s), charge transfer resistance (R_{ct}), and double-layer capacitance (C_{dl}), which shows good agreement with the experimental data (inset Fig. 3C). These results are consistent with the CV and LSV analyses, further confirming the improved electrochemical performance of the Co-MOF-modified electrode.

Fig. 3D represents the cyclic stability of Co-MOF/GCE at 0–1.3 V potential range at 0.5 V s^{-1}, showing that the oxidation peak currents follow a similar pattern and exhibit no significant deviation even after 25 cycles. Therefore, Co-MOF/GCE demonstrates improved stability.

The electrochemical analysis (CV, LSV, EIS) revealed that the as-synthesized Co-MOF contains redox-active Co^{2+}/Co^{3+} centers, which facilitate rapid electron transfer and enhance electrochemical response. Unlike redox-inactive MOFs (*e.g.*, Zn-MOF), the as-prepared Co-MOF exhibits superior charge-transfer kinetics due to its partially filled d-orbitals.[33] The outstanding electrochemical behavior of Co-MOF/GCE was further utilized in a nanozymatic biosensing application. For example, the nanozymatic activity of Co-MOF was measured under electrochemical conditions instead of a conventional microplate or microtube-based system. It is expected that the nanozymatic activity will be enhanced under electrochemical conditions (Fig. 4A).

The feasibility of the present experimental design is presented in Fig. 4B. A six-fold enhancement in nanozymatic activity was observed under electrochemical settings compared to the conventional assay. No noticeable nanozymatic peak in the absence of Co-MOF was observed, indicating the significance of Co-MOF in the nanozymatic reaction. Moreover, a significant decrease in detection time (from 30 minutes to 30 seconds) indicates that the proposed detection strategy offers better sensitivity in a shorter time.

As shown in Fig. 5A, the nanozymatic activity is enhanced in sodium acetate buffer (pH 5.6) compared to the PBS buffer (pH 7.5). The optimized reaction time is 30 seconds (Fig. 5B). The best concentration of TMB and Co-MOF in this study is 6 mM and 40 μg mL^{-1}, respectively (Fig. 5C and D)

The sensitivity of the present assay was compared with that of the conventional method for the detection of H_2O_2 in buffer solution. As shown in Fig. 6A, the detection range of H_2O_2 using the conventional method is 1–10 μM. However, a significantly lower detection range of H_2O_2 (0.1–1 μM) is achieved under electrochemical conditions, indicating the superiority and novelty of the current protocol (Fig. 6B). The calculated LOD is 32 nM. The proposed H_2O_2 sensing results are comparable with those from the recent studies and are summarized in Table 1.

The proposed assay was further extended for the detection of dopamine. As shown in Fig. 7A, an inverse relationship of dopamine concentration with the absorbance of nanozymatic activity was observed due to the inhibition of dopamine. The

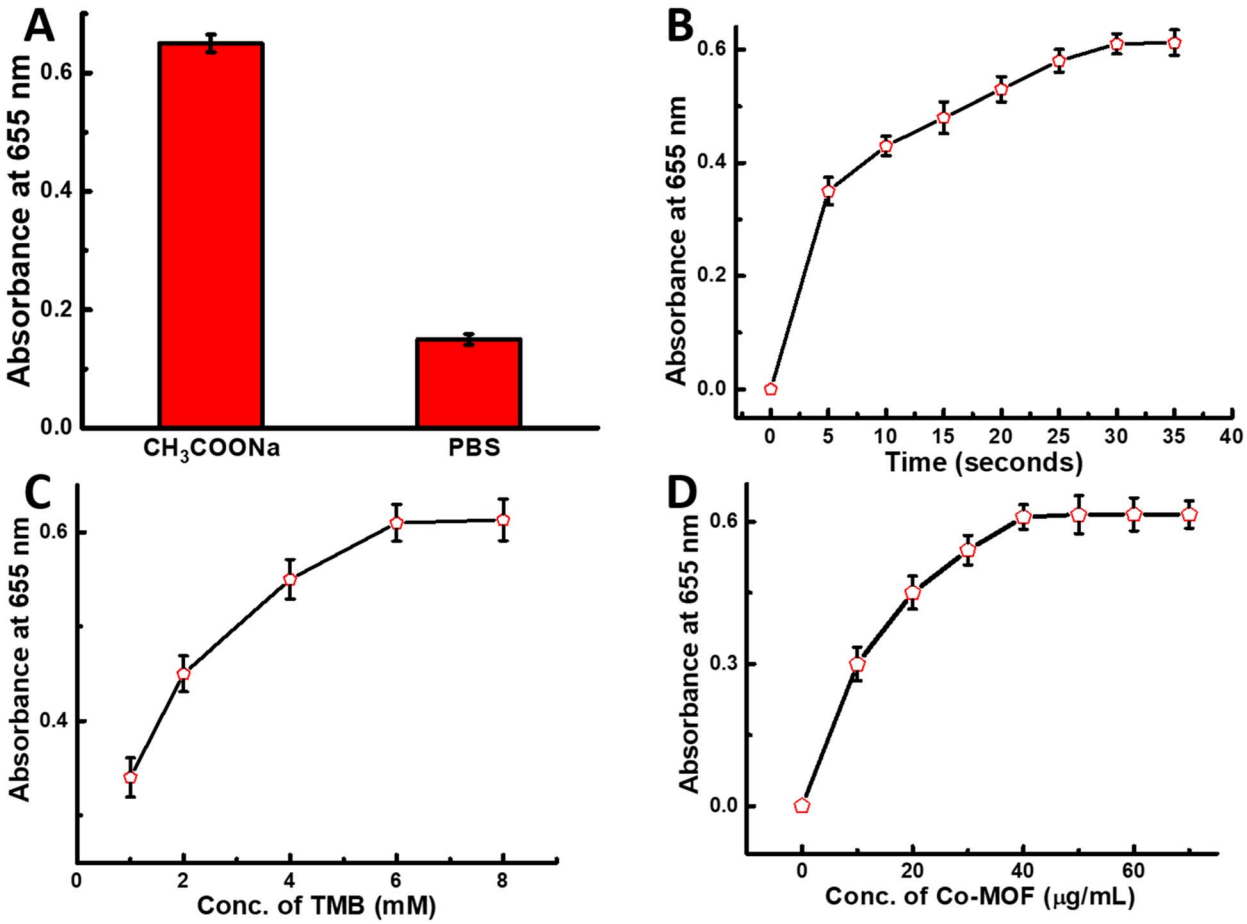

Fig. 5 Optimization of (A) buffer solution, (B) reaction time, (C) concentration of TMB and (D) concentration of Co-MOF.

suppression of the TMB oxidation was attributed to the depletion of hydroxyl radicals in the reaction with dopamine, thus reducing the number of available hydroxyl radicals in the reaction mixture for the oxidation of TMB.[38]

The detection range of dopamine using the present method is 2–12 μM, and the calculated LOD is 0.81 μM. Moreover, dopamine detection is highly specific since a very low absorbance was obtained for dopamine (12 μM) compared to other common interferent molecules with 10 times higher concentration of dopamine (120 μM) (Fig. 7B). Though norepinephrine and dopamine are structurally similar, most probably, the positive charge of dopamine strongly scavenges the negatively

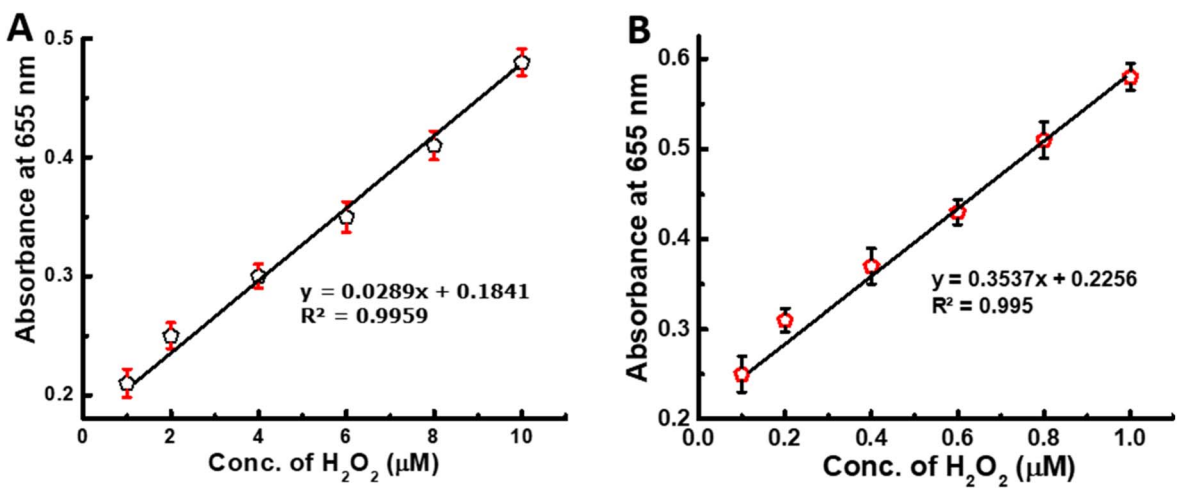

Fig. 6 Detection of H_2O_2 under conventional (A) and proposed (B) methods.

Table 1 Comparison of the LOD values of the present work with those of reported studies for H_2O_2 detection

		H_2O_2		
Nanomaterial	Method	Linear range (mM)	LOD (mM)	Ref
Cur-AuNPs	Colorimetric	0.05–0.5	0.05	34
Fe single-atom	Colorimetric	0.003–1	0.0013	35
Lys-Fe-NPs	Colorimetric	0.001–0.2	0.00051	36
MB-peptide	Colorimetric	0.00002–0.0002	0.000018	37
Co-MOF	Colorimetric	0.1–1	0.000032	Present study

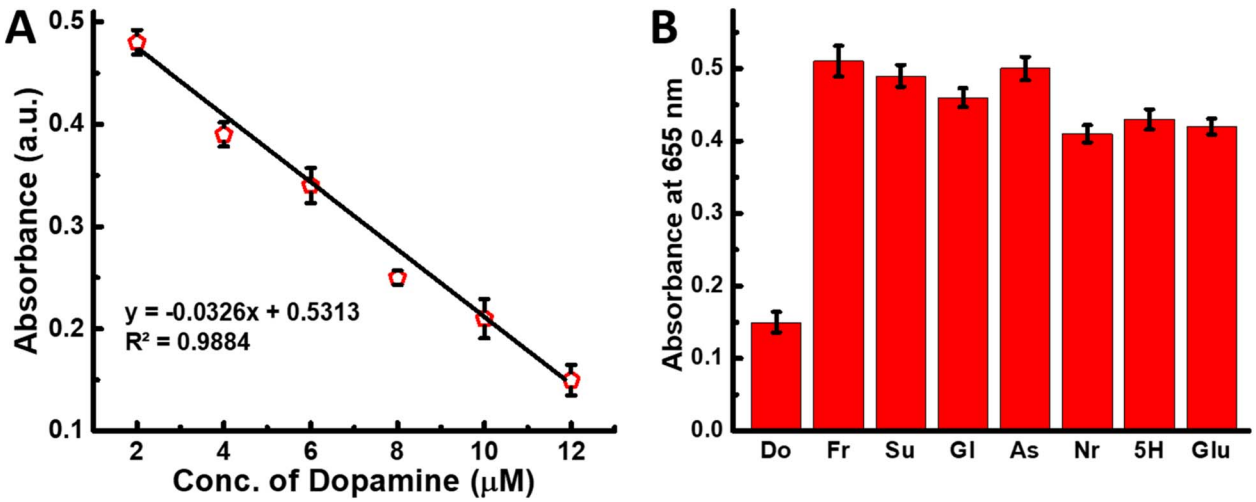

Fig. 7 Detection (A) and specificity (B) of dopamine using the proposed method (Do-Dopamine, Fr-fructose, Su-sucrose, Gl-glucose, As-ascorbic acid, Nr-norepinephrine, 5H-5-hydroxytryptamine, and Glu-glutathione).

charged hydroxyl radicals and significantly lowers the optical density (Table 2).

The sensitivity of the proposed electro-nanozymatic dopamine detection was comparable with that of recent studies, as summarized in Table 3. Most importantly, this assay could reduce the detection time significantly (from 30 min to 30 seconds).

Fig. 8 presents a cyclic voltammetry (CV) plot used to investigate the electrocatalytic activity of different combinations involving hydrogen peroxide (H_2O_2), 3,3′,5,5′-tetramethylbenzidine (TMB), and a cobalt-based metal–organic framework (Co-MOF). The black curve, representing H_2O_2 alone, shows a low current response, indicating poor electron transfer. The red curve of TMB alone exhibits a flat line with no significant redox peaks, confirming that TMB has negligible electrochemical activity under these conditions. Upon combining H_2O_2 with TMB (blue curve), the current increases moderately with the appearance of redox peaks, suggesting the oxidation of TMB by H_2O_2 but with limited reaction kinetics. Notably, the pink curve, which represents the combination of H_2O_2, TMB, and Co-MOF, shows a sharp rise in current, reaching approximately 600 μA at higher potentials, demonstrating a highly enhanced redox process and maximum electrocatalytic activity. In the final composite (pink curve), Co-MOF acts as a nanozyme *via* the catalytic decomposition of H_2O_2 into reactive oxygen species, which rapidly oxidize TMB.

Table 2 Comparison of LOD values of the present work with those reported for dopamine detection

		Dopamine		
Nanomaterial	Method	Linear range (mM)	LOD (mM)	Ref
BSA-Cu NPs	Colorimetric	0.001–0.03	0.000095	39
Pt@N	Colorimetric	0.001–0.1	0.000123	40
Fe_3O_4@C@AgNPs	Colorimetric	0.0005 0.08	0.00012	41
$CoFe_2O_4$	Colorimetric	0.05–0.8	0.01	42
GDY QDs	Colorimetric	0.02–0.1	0.00865	43
Co-MOF	Colorimetric	0.002–0.012	0.00081	Present study

Table 3 Analytical performance of the proposed assay in serum media

Labelled (μM)	Observed (μM)	Recovery (%)	RSD (%)
3	3.05	101.66	3.18
5	4.98	99.6	4.10
7	7.10	101.42	3.57
9	9.05	100.55	2.98
11	10.68	97.09	4.27

Additionally, Co-MOF provides a large surface area and abundant redox-active sites, facilitating fast electron transfer and significantly enhancing the electrochemical signal. This makes the Co-MOF-based composite an effective catalyst for H_2O_2 detection and TMB oxidation.

A comparison of the kinetic parameters is presented in the supporting document (Table S1) that reveals that the Co-MOF has relatively lower K_m values, indicating that it has a greater affinity for TMB and H_2O_2. The as-synthesized Co-MOF has the redox-active Co^{2+}/Co^{3+} centers and partially filled d-orbitals that facilitate rapid electron transfer, exhibiting superior charge transfer kinetics under the applied electrochemical force. In addition, the porous structure and high surface area of the synthesized Co-MOF provide abundant active sites and improved mass transport that significantly amplifies its catalytic performance. Moreover, the observed smaller V_{max} values for Co-MOF denote that the reaction rate was slower upon saturation with its substrate.

The analytical performance of the proposed dopamine assay was further examined in a simulated blood serum sample (BZ278, Biochemazone, Edmonton, Canada). The results are presented in Table 3 and reveals that the recovery percentage is in the range of 97.09–101.66 with a RSD value less than 5%. These findings strongly support the practical applicability of the proposed assay.

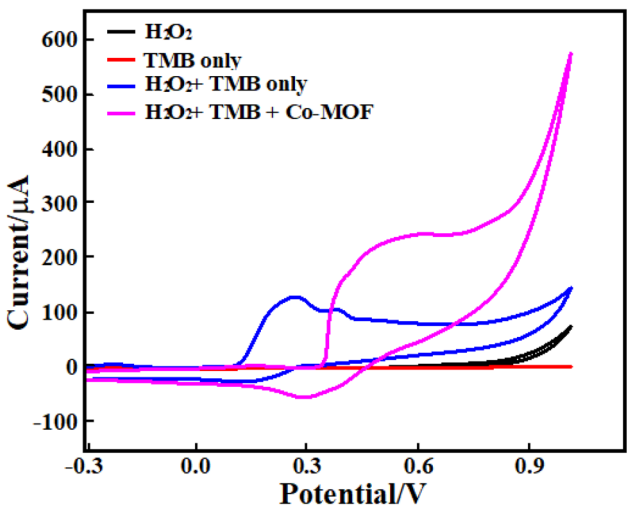

Fig. 8 CVs recorded for different composites in pH 7 PBS (0.01 M) at a scan rate of 0.5 V s^{-1} (*vs.* Ag/AgCl RE) on H_2O_2 (black curve), TMB (red curve), H_2O_2 + TMB (blue curve) and H_2O_2 + TMB + Co-MOF (pink curve) electrodes.

Conclusions

In this study, the electrochemical properties of Co-MOF were utilized to enhance its weak nanozymatic activity. At first, the environment-friendly Co-MOF was synthesized using the microwave method and characterized using FESEM, TEM and EDX. The as-synthesized Co-MOF has a granular pearl shape and exhibited higher electrochemical performance. The integration of electrochemically active Co-MOF with the nanozymatic activity produced a significantly enhanced nanozymatic activity, which was utilized for the detection of H_2O_2 and dopamine. The calculated LOD values for H_2O_2 and dopamine are 32 nM and 0.81 μM, respectively. Impressively, the detection time was reduced from 30 min to 30 seconds, which could facilitate rapid monitoring of large amounts of analytes with significantly shorter time. The present green synthesis of Co MOF, its integration with electrochemical settings to improve the nanozymatic activity and shorter bioanalytical detection time will promote their applications in multidisciplinary areas.

Conflicts of interest

The authors declare that they have no known competing financial interests or personal relationships that could have appeared to influence the work reported in this study.

Data availability

All data supporting the findings of this study are available within the article. Additional raw data can be provided by the corresponding author upon reasonable request.

Supplementary information (SI) is available. See DOI: https://doi.org/10.1039/d6ay00361c.

Acknowledgements

The authors would like to acknowledge the support from the Natural Sciences and Engineering Research Council of Canada in the form of Discovery Grants to ARR and SS (RGPIN-2019-07246 (https://www.sciencedirect.com/science/article/pii/S0026265X25006332) and RGPIN-2022-04988 (https://www.sciencedirect.com/science/article/pii/S0026265X25006332)). This work was also financially supported by the Ministry of Higher Education, Malaysia, for niche area research under the Higher Institution Centre of Excellence (HICoE) program (JPT(BKPI)1000/016/018/28 Jld.3(2) & NANO-CAT-2024B).

References

1 A. Portorreal-Bottier, S. Gutiérrez-Tarriño, J. J. Calvente, R. Andreu, E. Roldán, P. Oña-Burgos and J. L. Olloqui-Sariego, Enzyme-like activity of cobalt-MOF nanosheets for hydrogen peroxide electrochemical sensing, *Sens. Actuators, B*, 2022, **368**, 132129, DOI: 10.1016/j.snb.2022.132129.

2 B. Zhu, L. Zhu, T. Hou, K. Ren, K. Kang, C. Xiao and J. Luo, Cobalt Metal–Organic Frameworks with Aggregation-

Induced Emission Characteristics for Fluorometric/Colorimetric Dual Channel Detection of Nitrogen-Rich Heterocyclic Compounds, *Anal. Chem.*, 2022, **94**(9), 3744–3748, DOI: 10.1021/acs.analchem.1c05537.

3 R. M. A. Ismail, E. A. Enemose, M. Al-Jamal, S. K. Ramachandran, H. Al-Mattarneh and D. Gangodkar, Co-MoF Derived Colorimetric Sensors for Detection of Environmental Toxic Heavy Metal Analysis, *Adv. Sci. Technol.*, 2022, **117**, 43–49, DOI: 10.4028/p-6pqbv5.

4 D. Li, S. Zhang, X. Feng, H. Yang, F. Nie and W. Zhang, A novel peroxidase mimetic Co-MOF enhanced luminol chemiluminescence and its application in glucose sensing, *Sens. Actuators, B*, 2019, **296**, 126631, DOI: 10.1016/j.snb.2019.126631.

5 Z. Ma, Y.-S. Wang, B. Liu, H. Jiang and L. Xu, A Non–Enzymatic Electrochemical Sensor of Cu@Co–MOF Composite for Glucose Detection with High Sensitivity and Selectivity, *Chemosensors*, 2022, **10**(10), 416, DOI: 10.3390/chemosensors10100416.

6 B. S. Goud, G. Shin, S. P. Vattikuti, N. Mameda, H. Kim, G. Koyyada and J. H. Kim, Enzyme-integrated biomimetic cobalt metal-organic framework nanozyme for one-step cascade glucose biosensing via tandem catalysis, *Biochem. Eng. J.*, 2022, **188**, 108669, DOI: 10.1016/j.bej.2022.108669.

7 I. Strauss, A. Mundstock, M. Treger, K. Lange, S. Hwang, C. Chmelik, P. Rusch, N. C. Bigall, T. Pichler, H. Shiozawa and J. Caro, Metal–Organic Framework Co-MOF-74-Based Host–Guest Composites for Resistive Gas Sensing, *ACS Appl. Mater. Interfaces*, 2019, **11**(15), 14175–14181, DOI: 10.1021/acsami.8b22002.

8 S. R. Ahmed, M. Sherazee, S. Srinivasan and A. R. Rajabzadeh, Positively Charged Gold Quantum Dots: An Nanozymatic "Off-On" Sensor for Thiocyanate Detection, *Foods*, 2022, **11**, 1189, DOI: 10.3390/foods11091189.

9 S. R. Ahmed, A. G. Cardoso, S. Kumar, G. A. Ortega, S. Srinivasan, A. R. Rajabzadeh, Nanozymes in Biosensing and Bioimaging, In *Nanozymes*, CRC Press, 1st edn, 2021.

10 S. R. Ahmed, M. Sherazee, S. Srinivasan and A. R. Rajabzadeh, Nanozymatic Detection of Thiocyanate through Accelerating the Growth of Ultra-Small Gold Nanoparticles/Graphene Quantum Dots Hybrids, *Food Chem.*, 2022, **379**, 132152, DOI: 10.1016/j.foodchem.2022.132152.

11 S. R. Ahmed, G. A. Ortega, S. Srinivasan and A. R. Rajabzadeh, Strong Nanozymatic Activity of Thiocyanate Capped Gold Nanoparticles: An Enzyme–Nanozyme Cascade Reaction Based Dual Mode Ethanol Detection in Saliva, *New J. Chem.*, 2022, **46**(3), 1194–1202, DOI: 10.1039/D1NJ03648C.

12 S. R. Ahmed, R. Chand, S. Kumar, N. Mittal, S. Srinivasan and A. R. Rajabzadeh, Recent Biosensing Advances in the Rapid Detection of Illicit Drugs, *TrAC, Trends Anal. Chem.*, 2020, **131**, 116006, DOI: 10.1016/j.trac.2020.116006.

13 M. Liang and X. Yan, Nanozymes: From New Concepts, Mechanisms, and Standards to Applications, *Acc. Chem. Res.*, 2019, **52**(8), 2190–2200, DOI: 10.1021/acs.accounts.9b00140.

14 X. Ren, D. Chen, Y. Wand, H. Li, Y. Zhang, H. Chen, X. Li and M. Huo, Nanozymes-recent development and biomedical applications, *J. Nanobiotechnol.*, 2022, **20**(1), DOI: 10.1186/s12951-022-01295-y.

15 S. R. Ahmed, A. G. Cardoso, H. V. Cobas, P. Das, S. Srinivasan and A. R. Rajabzadeh, Graphdiyne quantum dots for H_2O_2 and dopamine detection, *ACS Appl. Nano Mater.*, 2023, **6**(10), 8434–8443, DOI: 10.1021/acsanm.3c00771.

16 S. R. Ahmed, J. Kim, T. Suzuki, J. Lee and E. Y. Park, Enhanced Catalytic Activity of Gold Nanoparticle-carbon Nanotube Hybrids for Influenza Virus Detection, *Biosens. Bioelectron.*, 2016, **85**, 503–508, DOI: 10.1016/j.bios.2016.05.050.

17 S. R. Ahmed, K. Takemeura, T. Li, N. Kitamoto, T. Tanaka, T. Suzuki and E. Y. Park, Size-Controlled Preparation of Peroxidase-like Graphene-gold Nanoparticle Hybrids for the Visible Detection of Norovirus-like Particles, *Biosens. Bioelectron.*, 2017, **87**, 558–565, DOI: 10.1016/j.bios.2016.08.101.

18 S. R. Ahmed, J. Kim, V. T. Tran, T. Suzuki, S. Neethirajan, J. Lee and E. Y. Park, In Situ Self-assembly of Gold Nanoparticles on Hydrophilic and Hydrophobic Substrates for Influenza Virus-sensing Platform, *Sci. Rep.*, 2017, **7**, 44495, DOI: 10.1038/srep44495.

19 S. R. Ahmed, J. Kim, T. Suzuki, J. Lee and E. Y. Park, Detection of Influenza Virus Using Peroxidase-Mimic of Gold Nanoparticles, *Biotechnol. Bioeng.*, 2016, **113**, 2298–2303, DOI: 10.1002/bit.25982.

20 D. Jiang, D. Ni, Z. T. Rosenkrans, P. Huang, X. Yan and W. Cai, Nanozyme: new horizons for responsive biomedical applications, *Chem. Soc. Rev.*, 2019, **48**(14), 3683–3704, DOI: 10.1039/C8CS00718G.

21 P. Wang, D. Min, G. Chen, M. Li, L. Tong and Y. Cao, Inorganic Nanozymes: Prospects for Disease Treatments and Detection Applications, *Front. Chem.*, 2021, **9**, DOI: 10.3389/fchem.2021.773285.

22 P. Wang, T. Wang, J. Hong, X. Yan and M. Liang, Nanozymes: A New Disease Imaging Strategy, *Front. Bioeng. Biotechnol.*, 2020, **8**, DOI: 10.3389/fbioe.2020.00015.

23 Z. Deng, H. Zhang, P. Yuan, Z. Su, Y. Bai, Z. Yin and J. He, Cobalt-Based Metal-Organic Framework Nanoparticles with Peroxidase-like Catalytic Activity for Sensitive Colorimetric Detection of Phosphate, *Catalysts*, 2022, **12**(7), 679, DOI: 10.3390/catal12070679.

24 Y. Guan, Y. Lu, J. Zhao, W. Huang and Y. Liu, Cobalt-based zeolitic imidazole framework incorporated with well-dispersed bimetallic nanoparticles/ions as a multifunctional nanozyme for the degradation of environmental pollutants and discrimination of various phenolic substances, *Chem. Eng. J.*, 2023, **465**, 142703, DOI: 10.1016/j.cej.2023.142703.

25 J. Feng, J. Tang, C. Jiang, C. Zhu, D. Wang and S. Tang, Bimetallic copper/cobalt-doped nanozyme based fluorescence and electrochemistry dual-modal sensor for

dopamine detection, *Microchem. J.*, 2026, **222**, 117147, DOI: 10.1016/j.microc.2026.117147.

26 G. Li, Y. Chen, F. Liu, *et al.*, Portable visual and electrochemical detection of hydrogen peroxide release from living cells based on dual-functional Pt-Ni hydrogels, *Microsyst. Nanoeng.*, 2023, **9**, 152, DOI: 10.1038/s41378-023-00623-y.

27 M. Sherazee, S. R. Ahmed, P. Das, S. Srinivasan and A. R. Rajabzadeh, Electrochemically Enhanced Peroxidase-like Activity of Nanohybrids for Rapid and Sensitive Detection of H_2O_2 and Dopamine, *Colloids Surf. A Physicochem. Eng. Asp.*, 2023, **679**, 132576, DOI: 10.1016/j.colsurfa.2023.132576.

28 D. B. Bailmare, B. V. Malozyomov and A. D. Deshmukh, Electrodeposition of porous metal-organic frameworks for efficient charge storage, *Commun. Chem.*, 2024, **7**, 178, DOI: 10.1038/s42004-024-01260-w.

29 N. K. Gupta, J. Bae and K. S. Kim, Metal organic framework derived NaCoxOy for room temperature hydrogen sulfide removal, *Sci. Rep.*, 2021, **11**(1), 14740.

30 Y. Xie, F. Lijiao, L. Wenbing, Z. Qin and H. Guolin, Synthesis of Mn/Co-MOF for effective removal of U (VI) from aqueous solution, *Particuology*, 2023, **72**, 134–144, DOI: 10.1016/j.partic.2022.03.004.

31 V. T. Nam, P. T. Ni, H. N. Thu, N. N. Mai, T. A. Dung, N. T. Thanh, T. Q. Tung, T. V. Hau and T. T. Thuy, Tuning the thermal and mechanical properties of poly (vinyl alcohol) with 2, 5-furandicarboxylic acid acting as a biobased crosslinking agent, *Polym. J.*, 2022, **54**, 335–343, DOI: 10.1038/s41428-021-00583-y.

32 X. Hu, W. Haoye, Q. Songya, S. Z. W. Jiajun, C. Kaixuan, L. Shuji, H. Xuan, L. Shiping and X. Aijuan, Co/C nanomaterial derived from Co metal–organic framework for oxygen evolution reaction, *Ionics*, 2022, **28**, 813–821, DOI: 10.1007/s11581-021-04376-4.

33 D. M. D'Alessandro, Exploiting redox activity in metal–organic frameworks: concepts, trends and perspectives, *Chem. Commun.*, 2016, **52**, 8957, DOI: 10.1039/c6cc00805d.

34 P. Sudhesh, S. Sruthi, M. Jose, K. Vyshnavi, P. Aiswarya and R. Manu, Naked eye detection of hydrogen peroxide via curcumin functionalised gold nanoparticles, *Sci. Rep.*, 2025, **15**, 16896, DOI: 10.1038/s41598-025-01613-y.

35 Y. Zhang, P. Zhao, C. Qiao, J. Zhao, Y. Liu, Z. Huang, H. Luo, C. Hou and D. Huo, Fe Single-Atom Nanozymes for Real-Time Dual Monitoring of H_2O_2 Released from Living Cells, *ACS Appl. Nano Mater.*, 2023, **6**(11), 9901–9909, DOI: 10.1021/acsanm.3c01791.

36 X. Hou, R. Wang, H. Zhang, M. Zhang, X. Qu and X. Hu, Iron-Coordinated L-Lysine–Based Nanozymes with High Peroxidase-like Activity for Sensitive Hydrogen Peroxide and Glucose Detection, *Polymers*, 2023, **15**(14), 3002, DOI: 10.3390/polym15143002.

37 M. Puiu, O.-M. Istrate, V. Mirceski and C. Bala, Ultrasensitive Detection of Hydrogen Peroxide Using Methylene Blue Grafted on Molecular Wires as Nanozyme with Catalase-like Activity, *Anal. Chem.*, 2023, **95**(44), 16185–16193, DOI: 10.1021/acs.analchem.3c02919.

38 M. N. Ivanova, E. D. Grayfer, E. E. Plotnikova, L. S. Kibis, G. Darabdhara, P. K. Boruah, M. R. Das and V. E. Fedorov, *ACS Appl. Mater. Interfaces*, 2019, **11**(25), 22102–22112, DOI: 10.1021/acsami.9b04144.

39 J. Xu, Z. Lv, H. Xu and Z. Mao, A sensitive dopamine colorimetric sensing platform based on Co_3ZnC/co/co-N-C nanozyme with high oxidase-like activity, *Microchemical*, 2025, **215**, 114361, DOI: 10.1016/j.microc.2025.114361.

40 T. Ma, X. Wang, X. Yang, Y. Mao and M. Li, Resin-Templated Synthesis of Platinum Nanozymes with Dual Oxidase and Peroxidase Activity for Dopamine Detection, *ACS Appl. Nano Mater.*, 2025, **8**(39), 18914–18923, DOI: 10.1021/acsanm.5c03316.

41 T. A. Melisew and R. Nicolette, Hendricks-Leukes, Silver nanoparticles loaded carbon-magnetic nanocomposites: A nanozyme for colorimetric detection of dopamine, *Spectrochim. Acta, Part A Mol. Biomol. Spectrosc.*, 2024, **322**, 124830, DOI: 10.1016/j.saa.2024.124830.

42 M. Marieeswaran and P. Panneerselvam, Self-signaling colorimetric sensor for selective detection of dopamine based on $CoFe_2O_4$ nanozyme accelerated dopamine polymerization, *Anal. Chim. Acta*, 2025, **1338**(8), 343596, DOI: 10.1016/j.aca.2024.343596.

43 S. R. Ahmed, A. G. Cardoso, H. V. Cobas, P. Das, A. Chen, S. Srinivasan, A. R. Rajabzadeh, *et al.*, Graphdiyne Quantum Dots for H_2O_2 and Dopamine Detection, *ACS Appl. Nano Mater.*, 2023, **6**(10), 8434–8443, DOI: 10.1021/acsanm.3c00771.